Check for updates

Advanced Functional Materials

ADVANCED FUNCTIONAL MATERIALS
www.afm-journal.de

RESEARCH ARTICLE OPEN ACCESS

Reversible Tuning of Multiple Molecular Kinking for Stem Cell Regulation In Vivo

Kanghyeon Kim[1] | Jeongah Shin[1] | Chowon Kim[1] | Honghwan Choi[2,3] | Dahee Kim[1] | Sungkyu Lee[1] | Choongmo Kang[1] | Hyunsik Hong[1] | Taehoon Ha[1] | Nayeon Kang[1] | Jungyeon Rhi[1] | Ramar Thangam[1] | Yuri Kim[1] | Jeongyun Heo[2,4,5] | Cheol Hwan Kwak[6] | Jangsun Hwang[7] | Daun Jeong[7] | Rasoul Moradi[8,9] | Sunghoon Hur[10,11,12] | Hyun-Cheol Song[1] | Hyun-Do Jung[13] | Min Jae Lee[14,15] | Rongqin Huang[16] | Pooyan Makvandi[17,18] | Yun Suk Huh[6] | Ji Hye Choi[7] | Wenguo Cui[19] | Sehoon Kim[2,3] | Heemin Kang[1,20]

[1]Department of Materials Science and Engineering, Korea University, Seoul, Republic of Korea | [2]Chemical and Biological Integrative Research Center, Korea Institute of Science and Technology, Seoul, Republic of Korea | [3]KU-KIST Graduate School of Converging Science and Technology, Korea University, Seoul, Republic of Korea | [4]Graduate Program in Innovative Biomaterials Convergence, Ewha Womans University, Seoul, Republic of Korea | [5]Basic Sciences Research Institute (Priority Research Institute), Ewha Womans University, Seoul, Republic of Korea | [6]NanoBio High-Tech Materials Research Center, Department of Biological Sciences and Bioengineering, Inha University, Incheon, Republic of Korea | [7]Department of Orthopedic Surgery, Korea University Anam Hospital, Seoul, Republic of Korea | [8]Department of Chemical Engineering, Khazar University, Baku, Azerbaijan | [9]Department of Mechanical and Aerospace Engineering, Samueli School of Engineering and Applied Sciences, University of California Los Angeles, Los Angeles, California, USA | [10]Electronic and Hybrid Materials Research Center, Korea Institute of Science and Technology (KIST), Seoul, Republic of Korea | [11]KIST-SKKU Carbon-Neutral Research Center, Sungkyunkwan University (SKKU), Suwon, Republic of Korea | [12]School of Advanced Materials Science and Engineering, Sungkyunkwan University (SKKU), Suwon, Republic of Korea | [13]Division of Materials Science and Engineering, Hanyang University, Seoul, Republic of Korea | [14]Department of Mechanical Engineering, Seoul National University, Seoul, Republic of Korea | [15]Materials Research & Engineering Center, Hyundai Motor Company, Hwaseong-si, Republic of Korea | [16]State Key Laboratory of Metabolic Dysregulation & Prevention and Treatment of Esophageal Cancer, Tianjian Laboratory of Advanced Biomedical Sciences, Academy of Medical Sciences, The Third Affiliated Hospital, Zhengzhou University, Zhengzhou, China | [17]Centre for Research Impact & Outcome, Chitkara College of Pharmacy, Chitkara University, Rajpura, Punjab, India | [18]University College, Korea University, Seoul, Republic of Korea | [19]Department of Orthopaedics Shanghai Key Laboratory For Prevention and Treatment of Bone and Joint Diseases, Shanghai Institute of Traumatology and Orthopaedics, Ruijin Hospital, Shanghai Jiao Tong University School of Medicine, Shanghai, China | [20]College of Medicine, Korea University, Seoul, Republic of Korea

Correspondence: Sehoon Kim (sehoonkim@kist.re.kr) | Heemin Kang (heeminkang@korea.ac.kr)

Received: 25 March 2026 | **Revised:** 8 August 2026 | **Accepted:** 12 August 2026

Keywords: ligand masking | molecular kink | multi-kink molecules | reversible photonic control | stem cell fate regulation

ABSTRACT

In the native extracellular matrix, collagen fibrils regulate stem cell fate and tissue regeneration by modulating the number of serial kinks via intramolecular kinking and unkinking, which affects integrin ligation. However, biomimetic materials composed solely of multi-kink-bearing molecules for dynamic regulation of ligand exposure remain limited. In this study, we designed materials composed solely of liganded multiple kink-bearing molecules with a tunable number of kink points (mono-kink, tri-kink, and penta-kink molecules), including flexible linkers and densely packed via intermolecular interactions, are designed. Near-infrared-upconverted ultraviolet light and visible light induce multiple kinking and unkinking of liganded multiple kink-bearing molecules conjugated to upconversion nanoparticle-coated materials, inducing kinked and unkinked states, respectively. Tri-kinking

Kanghyeon Kim, Jeongah Shin, Chowon Kim, Honghwan Choi and Dahee Kim contributed equally to this work.

This is an open access article under the terms of the Creative Commons Attribution-NonCommercial-NoDerivs License, which permits use and distribution in any medium, provided the original work is properly cited, the use is non-commercial and no modifications or adaptations are made.
© 2026 The Author(s). *Advanced Functional Materials* published by Wiley-VCH GmbH

and unkinking mediate the effective regulation of ligand masking and exposure, respectively, by modulating intermolecular interactions, while mono-kink and penta-kink molecules continuously expose the ligands regardless of their kinking/unkinking state. Tri-unkinking cyclically stimulates integrin ligation and focal adhesion-mediated stem cell mechanotransduction and differentiation in vivo, which are inhibited by tri-kinking. This study presents a newly developed reversibly switchable multi-kink molecule-conjugated surface for dynamic regulation of ligand exposure and stem cell responses, providing a useful modality for regulating cell–material interactions and stem cell fate in vivo.

1 | Introduction

Native molecules can dynamically form kinks through bending, which is regulated by intermolecular interactions, in vivo [1, 2]. Here, a "kink" refers to a bent or conformationally altered molecular motif that changes the spatial presentation or accessibility of a functional moiety. Such kinks determine the conformation of macromolecules, thus regulating their biological functions [3–6]. For example, the double helix structure of RNA exhibits a motif of kink-turns formed by intramolecular interactions and stabilized by metal ions [7]. These kink-turns bind to specific protein sites and mediate biological functions in vivo via 3D structural interactions [8, 9]. Dynein has a kink in its stalk that enables the molecule to move toward the minus end of microtubules [6]. In proteins, a proline residue can mediate reversible structural changes via photoisomerization between the *trans* and *cis* states, thus regulating biological functions such as signal transmission and enzymatic activity [10, 11]. Hence, to unravel and regulate cellular function in vivo, biomimetic materials [12], including molecules capable of reversible switching of the kinked state, are needed.

Kinks in extracellular matrix (ECM) molecules can regulate the binding of receptors to ligands, such as the Arg-Gly-Asp (RGD) motif, which mediates cell adhesion and tissue regeneration involving stem cell differentiation [13, 14]. The kinked structure of heparin sulfate, a glycosaminoglycan in the ECM, is governed by the flexibility of iduronic acid as well as ionic bonds and van der Waals interactions between protein and sugar molecules [15, 16], and regulates tissue regeneration [17]. Hyaluronic acid exhibits structural changes depending on the degree of kink formation, regulating cellular adhesion [18]. Laminin undergoes dynamic structural changes in kinks present in the integrin-binding site, regulating integrin ligation-mediated cellular adhesion [19]. Fibronectin contains RGD motifs that are hidden in the kinked state and exposed in the unkinked state induced through cellular traction force, thus modulating cellular adhesion [20]. Collagen can exhibit *cis* proline-mediated kinks [21] that mask integrin-binding sites [22], thus interfering with signal transmission in the ECM and inducing osteogenesis imperfecta, whereas collagen in the unkinked state promotes osteogenesis [23, 24]. Collagen fibrils show localized kinked structures, which mask integrin-binding sites and suppress cellular adhesion and tissue regeneration [25, 26]. Strikingly, collagen fibrils modulate the number of serial kinks in response to intramolecular kinking and unkinking to regulate the function of collagen bundles and tissues, such as bone and tendon [27–29]. Biomimetic materials capable of multiple molecular kinking and unkinking would reflect dynamic structural changes in ECM molecules, offering benefits in unraveling and regulating stem cell fate and tissue regeneration in vivo.

Biomaterials allowing control of the collective multiple kinking and unkinking dynamics can regulate ligand presentation, which emulates the dynamic ECM structure and function, and thus promote tissue regeneration [30–32]. Static liganded materials comprising mono-kink- and non-kink-bearing molecules have been used to fabricate DNA-functionalized liganded materials that exhibit unkinking-based binding site activation [33–35]. However, they do not allow dynamic and reversible modulation of kink structures in response to the constantly changing biological microenvironment. Dynamic materials that exhibit spatiotemporal changes in kink-bearing molecules under the control of various stimuli, including endogenous chemical stimuli [36–38] and exogenous stimuli such as spatially localizable light [39–45], have been designed. For example, dynamic materials comprising mono-kink- and non-kink-bearing molecules have been developed to regulate host-guest binding [40] and nanopore size [41] through light-controllable kinking and unkinking. Our group and others have developed dynamic stimuli-responsive materials based on mono-kink molecules and auxiliary non-kink-bearing background components to modulate the dynamic blocking [42], nanospacing [43], binding [44], stacking [45], and oscillation [46] of ligands. Although these systems have enabled dynamic control of specific molecular or cellular events, most reported kink-based platforms rely on a single kink point and have not been systematically connected to downstream stem cell mechanotransduction, osteogenic differentiation-associated responses, or in vivo outcomes. Therefore, a background component-free multi-kink molecule-conjugated surface, defined here as a surface composed of liganded multi-kink molecules without separate non-kink-bearing background components, could provide a useful platform for linking molecular kinking/unkinking, terminal ligand masking/exposure, and stem cell regulation.

In this study, we fabricated materials solely consisting of liganded multiple kink-bearing molecules with a tunable number of kink points (i.e., 1, 3, or 5 kink points) through a click reaction. Flexible linkers were incorporated between the molecules to facilitate the formation of densely packed structures via intermolecular interactions (π–π stacking, hydrogen bonds, and aromatic hydrogen bonds) and the reversible bending of the molecules (Figure 1a–c). Near-infrared light (980 nm)-upconverted ultraviolet light (365 nm) and visible light (448 nm) were used to cyclically induce multiple kinking and unkinking, respectively (Figure 2a). The multiple kink-bearing molecules were coupled to upconversion nanoparticle-coated materials that modulate RGD ligand presentation at the terminal functional group in the kinked and

16163028, 2026, 86, Downloaded from https://advanced.onlinelibrary.wiley.com/doi/10.1002/adfm.77914 by Hanyang University Library, Wiley Online Library on [24/11/2026]. See the Terms and Conditions (https://onlinelibrary.wiley.com/terms-and-conditions) on Wiley Online Library for rules of use; OA articles are governed by the applicable Creative Commons License

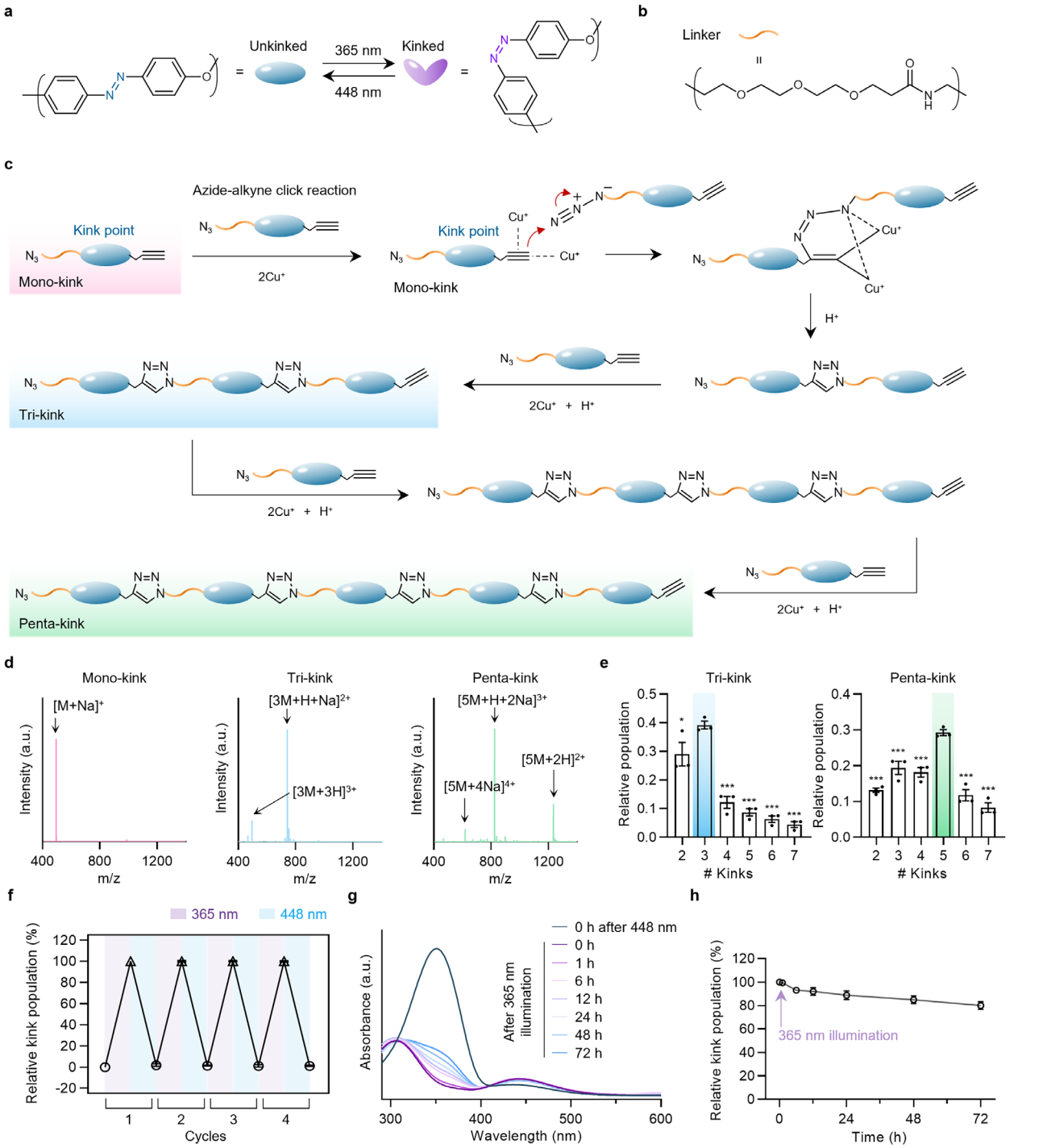

FIGURE 1 | Synthesis of multi-kink molecules with a tunable number of kink points for reversible kinking and unkinking. (a) Schematic representation of a molecular structure containing a single kink point that reversibly transition to the kinked state under 365 nm illumination and to the unkinked state under 448 nm illumination, respectively. (b) Schematic representation of the molecular linker connecting the kink points. (c) Multi-kink (tri-kink and penta-kink) molecules were synthesized from mono-kink molecules through a click reaction. Molecular length was controlled by adjusting the concentration of the mono-kink molecules during synthesis. (d) LC-HRMS spectra of multi-kink molecules. For qualitative analysis, mass spectra for mono-kink, tri-kink, and penta-kink molecules were selected at specific retention times of 6.50, 7.03, and 8.71 min, respectively. The prevalent m/z values corresponding to the different eluted compounds are indicated with arrows. (e) Distribution (relative populations) of the number of kinks in tri-kink and penta-kink molecules as determined with HPLC-UV. Asterisks indicate statistically significant differences with p-values (*$p < 0.05$ and ***$p < 0.001$). (f) Relative population of the kinked state in tri-kink molecules calculated based on the UV–vis absorption spectra in Figure S11. The graph shows the relative kink populations in tri-kink molecules after four cycles of sequential 448 nm (0.2 W/cm^2 for 1 min) and 365 nm (0.25 W/cm^2 for 1 min) illumination. Separate graphs for each illumination cycle are shown in Figure S11 in the Supporting Information. (g) UV–vis absorption spectra showing temporal variations in the tri-kink molecules after initial 448 nm illumination (0.2 W/cm^2 for 1 min) followed by 365 nm illumination (0.25 W/cm^2 for 1 min), and (h) corresponding calculation of the relative population of the kinked state (%) in the tri-kink molecules. The data are presented as mean ± standard error ($n = 3$ independent samples).

16163028, 2026, 86, Downloaded from https://advanced.onlinelibrary.wiley.com/doi/10.1002/adfm.77914 by Hanyang University Library, Wiley Online Library on [24/11/2026]. See the Terms and Conditions (https://onlinelibrary.wiley.com/terms-and-conditions) on Wiley Online Library for rules of use; OA articles are governed by the applicable Creative Commons License

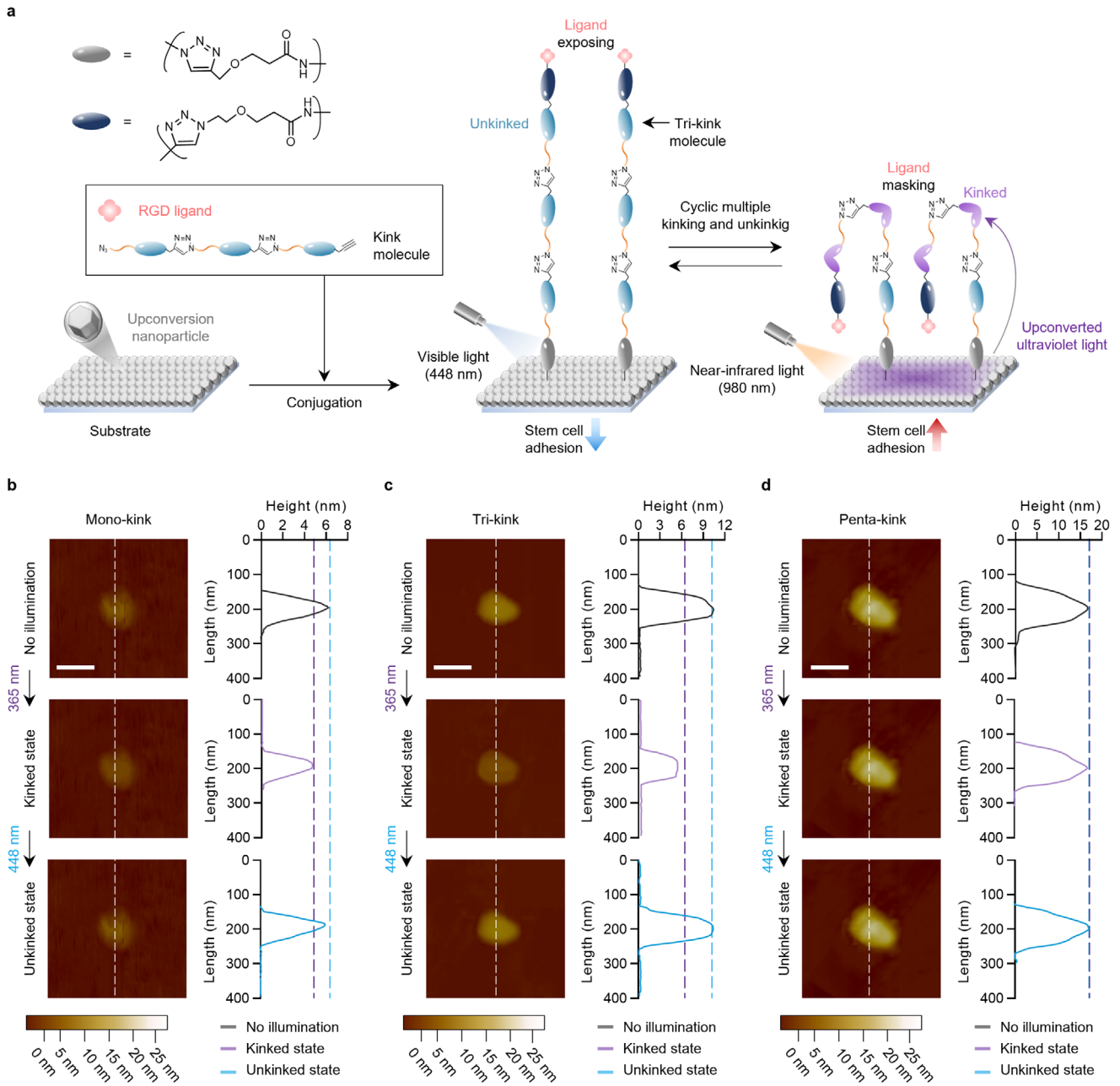

FIGURE 2 | Tri-kink molecules demonstrate the largest height change upon photoisomerization-induced transition between the unkinked and kinked states. (a) Tri-kink molecules exhibit reversible switching between ligand masking and exposure under 980 nm and 448 nm illumination, respectively, allowing for effective cell regulation. In-situ AFM images of a surface-bound (b) mono-kink molecule, (c) tri-kink molecule, and (d) penta-kink molecule demonstrating reversible height changes upon 365 nm (0.25 W/cm^2 for 10 min) and 448 nm (0.2 W/cm^2 for 10 min) illumination along with corresponding height profiles based on the AFM images. Scale bars: 100 nm.

unkinked state, thereby regulating integrin ligation-mediated cell adhesion.

This study presents newly developed dynamically regulatable multi-kink-bearing molecule-based materials for controlling ligand exposure and stem cell responses. Here, the terms "tri-kink" and "penta-kink" refer to narrowly dispersed oligomeric multi-kink molecules with average repeat numbers of approximately three and five, respectively. Notably, tri-kink molecules exhibited the largest difference in height between the aromatic hydrogen bond-dominant kinked state and the π–π stacking-dominant unkinked state, which effectively regulated illumination-induced ligand masking and exposing, respectively, while both states were stably maintained. In stark contrast, mono-kink and penta-kink molecules showed small height differences between the kinked and unkinked states, both of which exposed the ligands. This could be attributed to restricted photoisomerization with limited spatial freedom due to the short length in the mono-kink molecules and strong π–π stacking between the penta-kink molecules, yielding low intramolecular mobility. This demonstrates that materials utilizing mono-kink-bearing molecules cannot sufficiently bend to modulate ligand presentation and

16163028, 2026, 86, Downloaded from https://advanced.onlinelibrary.wiley.com/doi/10.1002/adfm.77914 by Hanyang University Library, Wiley Online Library on [24/11/2026]. See the Terms and Conditions (https://onlinelibrary.wiley.com/terms-and-conditions) on Wiley Online Library for rules of use; OA articles are governed by the applicable Creative Commons License

require background components to effectively harness kinking-based modulation of dynamic ligand presentation, which is consistent with recent findings [42–45].

We found that 980 nm light irradiation of the tri-kink molecules stimulated ligand exposure in the unkinked state, which cyclically promoted integrin-ligand binding and focal adhesion-mediated mechanosensing and osteogenic differentiation in stem cells in vitro and in vivo, whereas 448 nm illumination suppressed ligand exposure under multiple kinking and thus these stem cell responses. In contrast, mono-kink molecules readily exposed the ligands because of their short molecular length in the kinked and unkinked states, both of which activated the above stem cell responses. Penta-kink molecules caused unstable integrin-ligand binding because of their high molecular length and deactivated the stem cell responses despite the ligands being relatively exposed in both the kinked and unkinked states. In vivo maintenance of switchability between the kinked and unkinked states and upconverting functionality were demonstrated using fluorescence resonance energy transfer (FRET) imaging and photoluminescence, respectively, and were found to be required for effective stem cell regulation in vivo, without exerting systemic toxicity. Our aim in designing such background component-free switchable multi-kink materials was to enable novel modalities for dynamically regulating early stem cell responses and integrin-mediated mechanotransduction in vivo, with potential relevance for future regenerative applications.

2 | Results and Discussion

2.1 | Modulation of Molecular Length by Tuning the Number of Kink Points

We hypothesized that background component-free multiple molecular kinking and unkinking would modulate the conformation of surface-bound molecules to regulate terminal functional group exposure, thereby controlling cell adhesion. To test this hypothesis, we synthesized linear molecules harboring various numbers of kinks that can be remotely controlled with illumination. We first synthesized a mono-kink molecule, which was subsequently employed to produce tri-kink and penta-kink molecules, in which the kink points were linearly connected via triazole and oligo(ethylene glycol) linkers through click oligomerization (Figure 1). We introduced azobenzene as the kink point, which can be reversibly photoisomerized into the kinked state by 365 nm illumination and unkinked by 448 nm illumination, as the kink point (Figures 1a and S1). To achieve the linear arrangement of kink points via the click reaction, the mono-kink molecule was designed to contain an azide group and an alkyne group at the respective termini [47]. The tri-kink and penta-kink molecules with roughly three and five kink points, respectively, were synthesized through a Cu(I)-catalyzed alkyne-azide cycloaddition (CuAAC) click reaction. Molecular length was specifically controlled by using different concentrations of mono-kink molecules while keeping the reaction time constant (Figure 1c). The key benefits of the CuAAC click reaction [48, 49] are its high reaction efficiency and rate, allowing for facile molecular length tuning by simply adjusting the monomer concentration. The multi-kink (mono-kink, tri-kink, and penta-kink) molecules were functionalized with carboxylic acid for conjugation to the surface of underlying materials (Figures S2 and S3). Successful synthesis was validated using proton and carbon nuclear magnetic resonance (NMR), which revealed characteristic peaks for aromatic, propargylic, and azide-linked protons for the mono-kink molecule (Figures S4 and S5) and demonstrated the formation of a triazole group for the tri-kink and penta-kink molecules (Figures S6–S9).

We evaluated the synthesis of mono-kink, tri-kink, and penta-kink molecules using liquid chromatography coupled with high-resolution mass spectrometry (LC-HRMS). Their distribution and molecular length were quantitatively assessed using proton NMR and high-performance liquid chromatography coupled with ultraviolet absorption (HPLC-UV). For qualitative analysis, we performed an LC-HRMS screening of the mono-kink, tri-kink, and penta-kink molecules at specific time points corresponding to each unit and determined their relative population based on *m/z* values (Figure 1d and Table S1). HPLC-UV analysis revealed polydisperse molecular weight distributions, with an average molecular length of 3.23 for the tri-kink molecule and of 4.81 for the penta-kink molecule (Figure 1e). For the tri-kink molecule, the number-average molecular weight (M_n) was 1502, and the weight-average molecular weight (M_w) was 1,638, whereas for the penta-kink molecule, these values were 2235 and 2467, respectively. The polydispersity index values of 1.09 for the tri-kink molecule and 1.11 for the penta-kink molecule confirmed the narrow molecular weight distribution. Comprehensive proton NMR analysis was used to accurately determine the number of repeat units (Figure S8). The molecular length was determined by comparing the integration ratio of newly formed triazolyl proton (H_{13}) to the terminal propargylic proton (H_6), which appeared as a doublet, in the proton NMR spectra. The average ratios were 1.16 for the tri-kink molecule and 2.00 for the penta-kink molecule, corresponding to average molecular lengths of 3.31 and 5.01, respectively. These results confirmed the successful synthesis of the tri-kink and penta-kink molecules. Together, these results show that adjusting the concentration of mono-kink molecules during the CuAAC click reaction allows the effective incorporation of various numbers of kinks into the intramolecular chain, enabling controlled synthesis of tri-kink and penta-kink molecules with precisely regulated molecular lengths. The near-quantitative conversion of the terminal coupling reactions and the absence of unreacted functional groups were further validated by controlled spiking ^{1}H-NMR and FTIR analyses (Figure S10).

The multi-kink molecules exhibited maximum absorption at 315 nm in the kinked state and at 352 nm in the unkinked state. Reversible transition between the two states in the multi-kink molecules was confirmed using UV–vis absorption spectroscopy after four cycles of alternating illumination at 365 nm and 448 nm, demonstrating high cyclic reversibility (Figure 1f; Figures S11 and S12). Regardless of the number of kinks, the multi-kink molecules could be reversibly adjusted to the kinked or unkinked state by illumination at different wavelengths. The temporal stability of the multi-kink molecules in the kinked state was verified by monitoring the state of multi-kink molecules over 72 h using UV–vis spectroscopy after 365 nm illumination for 1 min to induce the kinked state (Figures 1g,h and S13). More than 80% of the kinked state was retained for 72 h, indicating the high thermal stability of the multi-kink molecules.

16163028, 2026, 86, Downloaded from https://advanced.onlinelibrary.wiley.com/doi/10.1002/adfm.77914 by Hanyang University Library, Wiley Online Library on [24/11/2026]. See the Terms and Conditions (https://onlinelibrary.wiley.com/terms-and-conditions) on Wiley Online Library for rules of use; OA articles are governed by the applicable Creative Commons License

2.2 | Dynamic Transition Between Kinked and Unkinked States via Illumination

The kinked state in the proposed multi-kink molecules is controlled by ultraviolet light, which can be harmful to patients [50] and exhibits low tissue penetration. To overcome these limitations, we introduced upconversion nanotransducers (UCNTs) to enable the use of near-infrared light. To improve the upconverting functionality of the UCNTs, the ytterbium and thulium dopant concentrations on the UCNT core ($NaYF_4$:Yb, Tm) were optimized, and a core–shell structure was generated through epitaxially aligned deposition of an $NaYF_4$ shell on the UCNT. The UCNT core–shell was coated with aminated silica to enhance the stability and conjugation of the multi-kink molecules.

The UCNT core was characterized by high resolution-transmission electron microscopy (HR-TEM) (Figure S14). The interior elemental distribution and uniform size of the UCNT core, UCNT core–shell, and silica-coated UCNT core–shell were analyzed using TEM, high-angle annular dark-field scanning TEM (HAADF-STEM), and elemental analysis (Figure S15). Dynamic light scattering revealed a stepwise increase in particle size throughout the preparation of the silica-coated UCNT core–shell structure (Figure S16).

Photoluminescence spectra revealed that the UCNP core emitted blue and ultraviolet light when excited with near-infrared light (980 nm) due to high-energy transfer from ytterbium to thulium [51, 52]. Ultraviolet emission from the UCNP was stronger than blue emission because of the shielding of surface defects through the formation of a shell structure on the UCNT core [53] and the suppression of surface quenching of the upconversion emission from the core by the inert $NaYF_4$ shell [54, 55]. Strong emission in the ultraviolet wavelength was maintained even after silica coating (Figure S17).

To verify the effects of the height and conformation of the multi-kink molecules on cellular regulation, the multi-kink molecules were coupled to aminated silica-coated UCNT core–shell substrates. To achieve uniform molecular height on the substrate, aminated UCNTs were coated in a monolayer on the bare substrate (Figure S18a). Under 980 nm excitation, the intensity ratio of ultraviolet to blue emission from the UCNT substrate was 3.19, indicating dominant upconverted ultraviolet emission at the substrate level (Figure S18b). We further calculated the integrated emission area over the ultraviolet region (320–380 nm) and blue region (430–480 nm), which yielded an integrated ultraviolet/blue emission ratio of 3.66. This result supports efficient 980 nm-to-ultraviolet upconversion at the substrate interface. The carboxylic group-ended mono- and multi-kink molecules were conjugated to the aminated UCNT substrate via the N-(3-dimethylaminopropyl)-N′-ethylcarbodiimide hydrochloride (EDC)/N-hydroxysulfosuccinimide (NHS) reaction. Subsequently, the activated NHS esters on the multi-kink molecules were decorated with amine group-bearing RGD, yielding liganded multi-kink molecule-conjugated UCNT substrate (Figure S19). Fourier-transform infrared spectra confirmed the binding between the multi-kink molecules and UCNT by the presence of Si-O-Si stretching [56] (1090 cm^{-1}) from the silica shell, N-H stretching [57] (3300–3500 cm^{-1}) from the aminated silica shell, and C = O stretching [58] (1740 cm^{-1}) from the multi-kink molecule, whereas the conjugation of RGD to multi-kink molecules was confirmed through the aryl hydroxyl peak [59] (1220 cm^{-1}) of RGD (Figure S20). Zeta potential analysis confirmed that the positively charged aminated UCNT exhibited a neutral surface charge upon conjugation with the NHS ester-ended multi-kink molecules, and a negative charge after further conjugation with the negatively charged RGD (Figure S21). These results suggested the successful construction of the liganded multi-kink molecule-conjugated UCNT substrate.

To verify whether the state of the multi-kink molecules conjugated to the UCNT substrate can be controlled with 448 nm visible light illumination and ultraviolet emission from the UCNT excited with 980 nm light, the substrate was illuminated with 448 and 980 nm light for 10 min and 1 min, respectively, for four cycles (Figure S22). After each illumination, UV–vis absorption was monitored. Upon 980 nm illumination, approximately 41% of the mono-kink molecules and 20% of the penta-kink molecules were transitioned to the kinked state. The tri-kink molecules showed the highest conversion efficiency, with approximately 72% adopting the kinked conformation. This distinct efficiency trend in the substrate-bound state is primarily governed by the balance between conformational freedom, intermolecular interaction, and steric confinement within the surface assembly.

As mono-kink and penta-kink molecules conjugated to the substrate showed low photoisomerization efficiency when switched from the unkinked to the kinked state, the thermal stability of tri-kink molecules conjugated to the substrate was examined using UV–vis spectroscopy (Figure S23). First, UV–vis absorption was measured after 448 nm illumination of the tri-kink molecule-conjugated UCNT substrate for 10 min to induce the unkinked state of the tri-kink molecules. Then, 980 nm light was applied for 10 min to induce the kinked state, and the state of the tri-kink molecules on the substrate was monitored for 72 h. After 72 h, approximately 87% of the tri-kink molecules on the substrate maintained the initial kinked state, whereas in solution, only approximately 80% of the initial kinked state was maintained for 72 h (Figure 1h). The enhanced stability on the substrate can be attributed to intermolecular interactions such as π–π interaction and hydrogen bonding [60] being facilitated by the decreased intermolecular distance between the tri-kink molecules conjugated on the substrate and is considered advantageous for effective switchable regulation of cell behavior on the substrate.

To investigate whether the hydrophilicity of the liganded multi-kink molecule-conjugated UCNT substrate depends on the state of the multi-kink molecules, cyclic changes in the contact angle were measured. After each illumination, changes in wettability were monitored in situ. The substrate exhibited increased hydrophilicity in the kinked state and decreased hydrophilicity in the unkinked state, consistent with a prior report [61]. The contact angle difference between 980 nm and 448 nm illumination was the largest in the tri-kink molecules, consistent with the UV–vis spectroscopy results (Figures S22 and S24). The contact angle remained below 25° in both the kinked and unkinked states, indicating the high hydrophilicity of the substrate [62] and implying that changes in hydrophilicity due to illumination would exert a negligible effect on cell adhesion.

16163028, 2026, 86, Downloaded from https://advanced.onlinelibrary.wiley.com/doi/10.1002/adfm.77914 by Hanyang University Library, Wiley Online Library on [24/11/2026]. See the Terms and Conditions (https://onlinelibrary.wiley.com/terms-and-conditions) on Wiley Online Library for rules of use; OA articles are governed by the applicable Creative Commons License

2.3 | Multiple Molecular Kinking and Unkinking Regulate the Degree of Ligand Exposure

Height changes in the surface-conjugated multi-kink molecules upon illumination at two wavelengths (365 and 448 nm) were analyzed using in situ atomic force microscopy (AFM) (Figure 2). Mono-kink molecules exhibited a maximum height of 6.2 nm in the absence of illumination. Their height slightly decreased to 4.7 nm upon light irradiation at 365 nm and subsequently increased to 6.0 nm when irradiated with 448 nm light (Figure 2b). Tri-kink molecules had a height of 10.4 nm in the absence of light, which significantly decreased to 5.5 nm upon 448 nm illumination and returned to 10.4 nm upon subsequent 365 nm illumination (Figure 2c). Penta-kink molecules had an initial height of 17.1 nm, which only slightly decreased to 16.9 nm after 448 nm illumination and slightly increased to 17.1 nm following 365 nm illumination (Figure 2d). These results were consistent with the UV–vis absorption data (Figure S22) and contact angle measurements (Figure S24), highlighting efficient state changes in the tri-kink molecules in contrast to limited state changes in the mono-kink and penta-kink molecules upon illumination. All multi-kink molecules showed a homogeneous configuration and consistent surface roughness regardless of the kinked or unkinked state (Figure S25). Based on these findings, we hypothesize that photoisomerization to the kinked state may be hampered in the mono-kink molecules due to the limited spatial freedom because of their short length and in the penta-kink molecules because of strong intermolecular interactions between penta-kink molecules with long molecular length.

To elucidate how light-induced multiple kinking and unkinking modulate the degree of ligand exposure and changes in intermolecular interactions in the multi-kink molecules, we performed molecular simulations using simple models of each of the multi-kink molecules constructed using the semi-empirical optimization method (Figure S26a–e). As shown in Figure S26b, mono-kink molecules, because of their relatively short length, allowed the ligands to remain readily exposed to cells even in the kinked state, with comparable heights of 49.1 and 50.5 Å in the kinked and unkinked state, respectively. In contrast, tri-kink molecules masked the ligands upon photoisomerization as the two kinks distal from the anchoring site transitioned into the kinked state, whereas the kink proximal to the anchoring site remained in the unkinked state, exhibiting a significant height change from 105.3 to 46.6 Å (Figure S26c, e). Notably, interactions between the molecular chain and the ligand led to an increased number of aromatic hydrogen bonds in the kinked state, suggesting that these interactions contributed to the stable maintenance of the ligand-masking conformation (Figure S26b,e). These findings corroborate that materials utilizing mono-kink-bearing molecules cannot sufficiently bend to modulate ligand presentation and require background molecules for kinking-based modulation of dynamic ligand presentation [42–45].

Penta-kink molecules in the unkinked state exhibited stronger intermolecular interactions than mono-kink and tri-kink molecules in the unkinked state, particularly extensive π–π stacking, resulting in restricted intramolecular mobility (Figure S26d,e). Consequently, photoisomerization to the kinked state was hindered in the penta-kink molecules, with only the kink point most distal from the anchoring site converting to the kinked state, which still exposed the ligands, accompanied by a small height decrease from 157.9 to 146.9 Å. The heights of the multi-kink molecules derived from the simulation were consistent with those obtained with in situ AFM (Figure 2), indicating successful simulation of the multi-kink molecules on the surface and ensuring reliable prediction of their molecular conformation. These results suggest that the tri-kink molecule may be the most advantageous for effective cell regulation, with the largest differences in height and intermolecular interactions between the kinked and unkinked states, resulting in illumination-induced ligand masking and exposure, respectively, while both states are stably maintained through different types of intermolecular interactions.

We used several strategies to increase the stability of the kinked and unkinked states. The triazole rings generated via alkyne–azide cycloaddition conferred a π-electron-rich character along the kink-bearing molecular backbone, facilitating lateral π–π stacking between aromatic rings to stabilize the multi-kink molecules. Hydrogen bonds between amide groups reinforced the intermolecular interactions, improving the structural integrity of the multi-kink molecules. To obtain linear multi-kink molecules, oligo(ethylene glycol) spacers were incorporated to connect the hydrophobic azobenzene units, enhancing overall hydrophilicity and rendering the structure suitable for biocompatible applications [63]. These flexible spacers provided rotational freedom and conformational flexibility to the kink points, thereby improving the efficiency of collective photoisomerization of the tri-kink molecules. This contrasts with conventional materials, in which rigid packing and strong intermolecular interactions often limit conformational transitions [64]. The kink points were sequentially connected to form continuous molecular backbones, fostering cooperative interactions among adjacent chains to yield densely packed molecules and thus enhance the stability of each state.

2.4 | Multiple Unkinking of Tri-Kink Molecules Effectively Regulates Stem Cells

Depending on the conformation of the multi-kink molecules, ligands can be either exposed or masked, potentially regulating the focal adhesion of stem cells. To test this, we cultured stem cells on liganded multi-kink molecule-UCNT substrates and illuminated them (or not, as a control) with 980 nm or 448 nm light (Figure 3a,b; Figures S27 and S28).

Stem cell adhesion on the multi-kink molecules was evaluated using immunofluorescence staining: promotion of stem cell adhesion was evaluated based on an increased number of paxillin clusters (indicating focal adhesion complexes), increased cell density, increased average cell area, and decreased axial ratio, whereas suppressed stem cell adhesion was determined as opposite changes in these parameters. On mono-kink molecules, stem cells adhered effectively regardless of the presence or absence of illumination or its wavelength. In contrast, on the penta-kink molecules, stem cell adhesion was relatively suppressed

16163028, 2026, 86, Downloaded from https://advanced.onlinelibrary.wiley.com/doi/10.1002/adfm.77914 by Hanyang University Library, Wiley Online Library on [24/11/2026]. See the Terms and Conditions (https://onlinelibrary.wiley.com/terms-and-conditions) on Wiley Online Library for rules of use; OA articles are governed by the applicable Creative Commons License

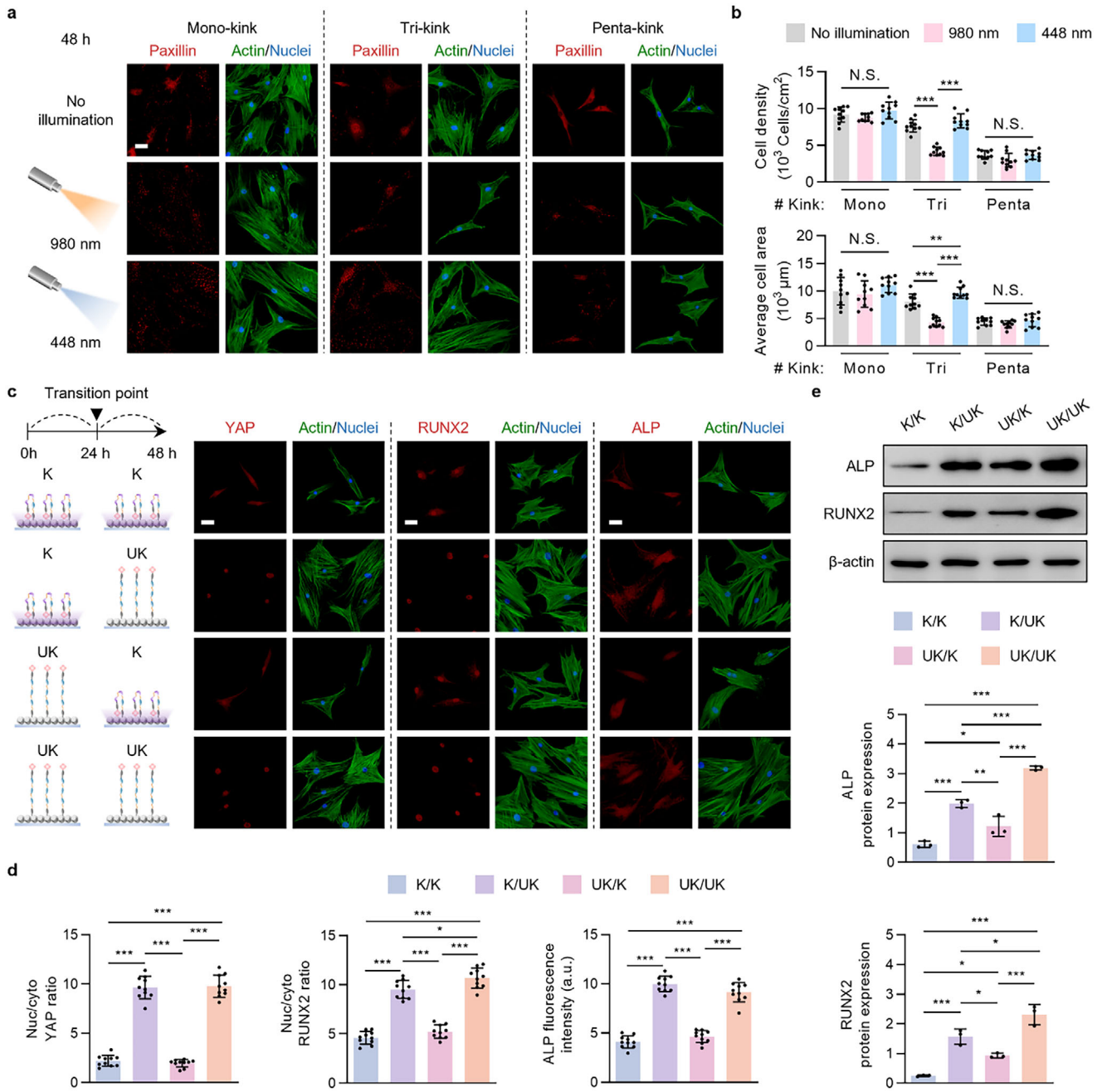

FIGURE 3 | Light-controlled multiple unkinking facilitates ligand exposure, which reversibly activates stem cell adhesion-mediated mechanotransduction and differentiation. (a) Immunofluorescence images of paxillin, actin, and nuclei of stem cells after 48 h of culturing on liganded multi-kink (mono-kink, tri-kink, and penta-kink) molecule-conjugated UCNT substrate and (b) quantification of the density and average area of stem cells based on the images. At 0 h and every 12 h after cell plating, substrates in the "980 nm" and "448 nm" groups were illuminated with 980 nm (1 W/cm^2 for 1 min) and 448 nm (0.2 W/cm^2 for 10 min) light, respectively. Cells in the "No illumination" group did not receive illumination. Scale bar: 50 μm. The data are presented as mean ± standard error ($n = 10$ randomly selected images from two independent substrates). (c) Immunofluorescence images of YAP, actin, and nuclei of stem cells after 48 h, and of RUNX2 or ALP along with actin and nuclei of stem cells after 72 h of culturing on liganded tri-kink molecule-conjugated UCNT substrates and (d) quantification of the nuclear/cytoplasmic (Nuc/cyto) YAP ratio, nuclear/cytoplasmic (Nuc/cyto) RUNX2 ratio, and ALP fluorescence intensity based on the images. The data are presented as mean ± standard error ($n = 10$ randomly selected images from two independent substrates). Scale bar: 50 μm. (e) Western blot images of ALP, RUNX2, and β-actin, and quantification of protein levels normalized to β-actin expression. Substrates were illuminated with 980 nm or 448 nm every 12 h, either with the same wavelength repeated ("K/K" and "UK/UK" groups) or with the wavelength switched at the midpoint of the 24 h culture period and continued every 12 h thereafter ("K/UK" and "UK/K" groups). The data are presented as mean ± standard error ($n = 3$ independent samples). Asterisks indicate statistically significant differences with p-values (*$p < 0.05$, **$p < 0.01$, and ***$p < 0.001$), while N.S. represents statistically non-significant differences.

16163028, 2026, 86, Downloaded from https://advanced.onlinelibrary.wiley.com/doi/10.1002/adfm.77914 by Hanyang University Library, Wiley Online Library on [24/11/2026]. See the Terms and Conditions (https://onlinelibrary.wiley.com/terms-and-conditions) on Wiley Online Library for rules of use; OA articles are governed by the applicable Creative Commons License

regardless of the illumination wavelength or presence/absence. Notably, in the kinked state induced by 980 nm irradiation, stem cell adhesion was further inhibited compared to that in the unkinked state under 448 nm illumination or in the absence of illumination. Strikingly, the tri-kink molecules were capable of effective regulation of cell adhesion in response to illumination: stem cell adhesion was relatively suppressed in the kinked state and relatively promoted in the unkinked state. These findings demonstrate that the tri-kink molecules feature ligand masking in the illumination-induced kinked conformation, hindering integrin binding and suppressing cell adhesion, as supported by the expression patterns of integrin β1 and talin (a focal adhesion protein) (Figures S29 and S30) [65–67].

As for the mono-kink molecules, their short molecular length likely prevented sufficient ligand masking, although the kinked state was fully induced by ultraviolet light emitted from the UCNTs under 980 nm excitation, facilitating ligand exposure but not suppressing stem cell adhesion. In the case of the penta-kink molecules, strong intermolecular interactions may have limited the conversion to the kinked state under 980 nm excitation. Furthermore, because of the instability of integrin-ligand binding in the relatively long penta-kink molecule [68–70], the ligands could have remained partially exposed even in the kinked state, leading to consistent deactivation of stem cell adhesion regardless of the excitation wavelength (980 nm *vs*. 448 nm) (Figure 3b). These findings collectively suggest that the tri-kink molecules demonstrate promising potential for stem cell adhesion regulation using illumination. Consistently, correlation analysis showed that molecular systems exhibiting larger light-responsive AFM height changes also displayed greater differences in integrin β1 recruitment and focal adhesion formation, supporting that light-induced unkinking/kinking modulates terminal ligand exposure or masking, which is reflected by changes in molecular height and stem cell adhesion responses (Figure S31).

To evaluate the effects of the system components, including the tri-kink molecules, ligands, and UCNTs, on stem cell adhesion, a series of control experiments, consecutively eliminating each of the components, were conducted. In the absence of the tri-kink molecules, UCNTs, or cell-adhesive ligands on the tri-kink molecules, stem cell adhesion was not maintained and thus not regulatable by 980 and 448 nm illumination, as evidenced by the insignificant differences in the adhesion parameters analyzed among the treatment groups (Figures S32–S34). Replacing the photoisomerizable tri-kink structure (conjugated to cell-adhesive ligands) with polyethylene glycol of similar molecular length but lacking kink points promoted stem cell adhesion regardless of the illumination wavelength or presence/absence (Figure S35). These results indicated that all components (tri-kink molecules, UCNTs, and ligands) are crucial for regulating stem cell adhesion through illumination-induced switching between multiple kinking and unkinking. Immunofluorescence staining and quantitative analysis showed that the 980 nm illumination-induced kinked state of the tri-kink molecules significantly suppressed the nuclear translocation of YAP and TAZ mechanotransducers, as indicated by lower nuclear/cytoplasmic YAP and TAZ immunofluorescence ratios compared to the unkinked state induced by 448 nm or no illumination (Figure S36). Osteogenic differentiation marker expression was significantly reduced in the kinked state compared to the unkinked state, as shown by the reduced nuclear/cytoplasmic RUNX2 immunofluorescence ratio and decreased alkaline phosphatase (ALP) and osteocalcin fluorescence intensities (Figure S37). In summary, the tri-kink molecules can regulate stem cell adhesion, mechanosensing, and osteogenic differentiation through multiple kinking and unkinking induced by illumination. These findings are consistent with previous reports showing that mechanosensing-mediated osteogenic differentiation is closely linked to focal adhesion assembly, actin cytoskeletal organization, and cytoskeletal force transmission [71, 72].

2.5 | Multiple Unkinking-Mediated Ligand Exposure Reversibly Stimulates Mechanotransduction-Mediated Stem Cell Differentiation

Temporal regulation of stem cell adhesion, mechanosensing, and osteogenic differentiation [73] is crucial for effective tissue regeneration. To verify the potential use of multi-kink molecules to this end, illumination-induced ligand exposure and masking in the tri-kink molecules were controlled in a time-dependent manner in a stem cell culture environment. Stem cells were cultured on the liganded tri-kink molecule-conjugated UCNT substrate, which showed high potential for stem cell regulation through illumination-induced molecular conformational changes. To induce the kinked state ("K") that masked the ligands, the substrate was illuminated with 980 nm, triggering the emission of upconverted UV light. To induce the unkinked state ("UK") that exposed the ligands, it was illuminated with 448 nm. Stem cells were cultured for 48 h, with illumination applied every 12 h. In the switching groups, the wavelength was changed at 24 h and subsequently applied every 12 h. Cells were collected at 24 and 48 h to assess the time-resolved effects of the controlled kinked state on the stem cells (Figure S38).

Immunofluorescence staining revealed that illumination after 24 h of cell culture dominantly regulated stem cell adhesion. Ligand masking induced by 980 nm illumination at 24 h (K/K and K/UK) significantly suppressed stem cell adhesion, whereas 448 nm-induced ligand exposure at this time point (UK/K and UK/UK) stimulated stem cell adhesion. After 48 h, sustained 980 nm illumination (K/K) significantly suppressed stem cell adhesion through ligand masking, whereas the maintenance of 448 nm illumination (UK/UK) promoted stem cell adhesion by maintaining ligand exposure. Strikingly, stem cell adhesion initially suppressed by ligand masking during the first 24 h was significantly enhanced through subsequent ligand exposure in the second 24 h (K/UK). Conversely, stem cell adhesion promoted by initial ligand exposure was greatly suppressed when followed by ligand masking in the second phase (UK/K). "UK" led to a higher cell density, average cell area, and focal adhesion number, and a lower cell axial ratio than "K" at each time point, demonstrating effective temporal regulation of stem cell adhesion through ligand exposure. In addition to regulating ligand masking/exposure, these light-induced changes in ligand accessibility may alter effective integrin–ligand coupling, focal adhesion-mediated force transmission, and local mechanical cues at the cell–material interface. Because local matrix mechanics and stiffness-dependent cues are known to strongly influence cellular functions and differentiation-associated responses [74],

16163028, 2026, 86, Downloaded from https://advanced.onlinelibrary.wiley.com/doi/10.1002/adfm.77914 by Hanyang University Library, Wiley Online Library on [24/11/2026]. See the Terms and Conditions (https://onlinelibrary.wiley.com/terms-and-conditions) on Wiley Online Library for rules of use; OA articles are governed by the applicable Creative Commons License

such changes may contribute to the observed temporal regulation of stem cell adhesion, mechanosensing, and osteogenic differentiation-associated responses.

Focal adhesion-mediated stem cell mechanosensing and osteogenic differentiation showed similar reversible patterns as cell adhesion (Figures 3c–e and S39) under the control of 980 and 448 nm illumination. The state of the tri-kink molecules in the second half of the culture period determined stem cell mechanosensing and osteogenic differentiation. Immunofluorescence staining showed that the kinked (K/K and UK/K) or unkinked (K/UK and UK/UK) state in the latter half of culture, respectively significantly suppressed and stimulated the nuclear translocation of the mechanotransducer YAP (Figure 3c,d). The osteogenic markers RUNX2 and ALP showed similar patterns (Figure 3c,d), which were confirmed by western blotting and quantitative PCR results (Figures 3e and S39). Continuous 980 nm illumination throughout culture resulted in the highest expression of the osteogenic differentiation markers, whereas persistent 448 nm illumination induced their lowest expression. Switching from 980 to 448 nm mid-culture induced a higher level of osteogenic differentiation than switching from 448 to 980 nm, indicating that the degree of ligand exposure in the later stages of cell culture dominates the regulation of stem cell differentiation.

Integrin-ligand binding activates p-FAK and RhoA-associated cytoskeleton regulation [71], thus regulating stem cell mechanosensing and osteogenic differentiation. Specific inhibitors were employed to verify the regulation of stem cell mechanosensing dependent on ligand exposure and masking by illumination-induced conformational changes in the tri-kink molecules (Figure S40). The addition of inhibitors of F-actin polymerization (cytochalasin D), myosin II (ML-9), or Rho-associated protein kinase (Y27632) during stem cell culture on the liganded tri-kink molecule-UCNT substrate consistently suppressed the translocation of the mechanotransducer YAP in ligand-exposed groups (K/UK and UK/UK), suggesting that focal adhesion-mediated stem cell mechanosensing was induced by the ligands exposed on the liganded tri-kink molecule-UCNT substrate. Complete ligand masking and exposure mediated by illumination-induced conformational changes were confirmed through empirical simulations and AFM (Figures 2 and S26). In addition, reversible ligand masking and exposure by light on liganded tri-kink molecule-UCNT substrate were confirmed over multiple cycles (Figure S22). Together, the results suggest that cyclic ligand masking and exposure enable the dynamic control of stem cell adhesion-mediated mechanosensing and differentiation.

2.6 | Light-Controlled Reversible Multiple Kinking and Unkinking In Vivo

Remote control of cellular responses in the in vivo microenvironment is advantageous for the spatiotemporal regulation of tissue regeneration. The tissue-regenerative potential of ligand masking and exposure of the liganded kink-molecules on UCNTs was assessed using an in vivo model. A liganded tri-kink molecule-UCNT substrate was implanted subcutaneously into the back of live mice and seeded with stem cells. Immediately and 3 h after implantation, 980 or 448 nm illumination was applied to the substrate at a 3 cm distance to control reversible molecular multi-kinking in vivo. At 6 h after implantation, the substrate was collected from the mice and used for immunofluorescence staining (Figure 4a,b; Figures S41 and S42).

Immunofluorescence staining of RUNX2 in HuNu-positive cells (HuNu: human nuclear antigen) showed that continuous ligand exposure (UK/UK) strongly stimulated stem cell osteogenic differentiation as indicated by the high nuclear/cytoplasmic RUNX2 immunofluorescence ratio (Figures 4a and S41). Ligand exposure during the second phase (K/UK) of cell culture promoted osteogenic differentiation more effectively than exposure during the initial phase (UK/K). In contrast, ligand masking throughout (K/K) or in the second phase (UK/K) suppressed osteogenic differentiation. Despite the relatively short post-implantation period, ligand exposure and masking in the second phase played a critical role in regulating stem cell fate. Furthermore, ligand exposure during the second phase (K/UK and UK/UK) stimulated focal adhesion-mediated stem cell mechanotransduction as evidenced by the significantly increased cell density, average cell area, and focal adhesion number, and lower cell axial ratio and YAP translocation compared with those upon ligand masking during the second phase (K/K and UK/K) (Figures 4a,b and S42). Consistent with the in-vitro results (Figure 3; Figures S38 and S39), these results indicated that illumination-induced ligand exposure and masking on the liganded multi-kink molecule-conjugated UCNTs can regulate focal adhesion-mediated stem cell differentiation in vivo.

To assess the in vivo stability of the multi-kink molecule-conjugated UCNTs, a fluorescent dye was conjugated to the multi-kink molecules instead of the ligand (Figure S43). A fluorescently labeled tri-kink molecule-conjugated UCNT substrate was implanted into live mice as described above. The fluorescence signal-to-background ratio for the fluorescently labeled tri-kink molecule-conjugated UCNT substrate was sustained for up to 3 weeks after substrate implantation, suggesting the long-term stability of the multi-kink molecules in vivo. The substrates were retrieved from the mice and subjected to SEM and photoluminescence analyses. The morphology of the monolayer of UCNTs on the substrate was maintained after 7 days of implantation (Figure 4c). The ratio of upconverted UV light to blue light remained stable over 3 weeks (Figure 4d,e). These results collectively suggest that the kinked state on the UCNT substrate was selectively achievable in vivo for up to 3 weeks post-implantation.

Given the demonstrated long-term in vivo stability of the tri-kink molecules and UCNTs, the feasibility of illumination-based control of the molecular conformation of the tri-kink molecules on the UCNT substrate in vivo was examined using fluorescence resonance energy transfer (FRET) imaging. The acceptor (Cy7) was bound to the UCNT surface, whereas the donor (Cy5.5) was conjugated to the distal end of the tri-kink molecules on the UCNT substrate (Figure 4f). In the unkinked state, the tri-kink molecules had a height of approximately 10 nm, leading to a greater donor–acceptor distance and lower FRET signal intensity than in the kinked state of approximately 5 nm height [75]. Cy5.5-tri-kink molecule-conjugated Cy7-UCNT substrate was implanted in live mice, and the FRET signal intensity

16163028, 2026, 86, Downloaded from https://advanced.onlinelibrary.wiley.com/doi/10.1002/adfm.77914 by Hanyang University Library, Wiley Online Library on [24/11/2026]. See the Terms and Conditions (https://onlinelibrary.wiley.com/terms-and-conditions) on Wiley Online Library for rules of use; OA articles are governed by the applicable Creative Commons License

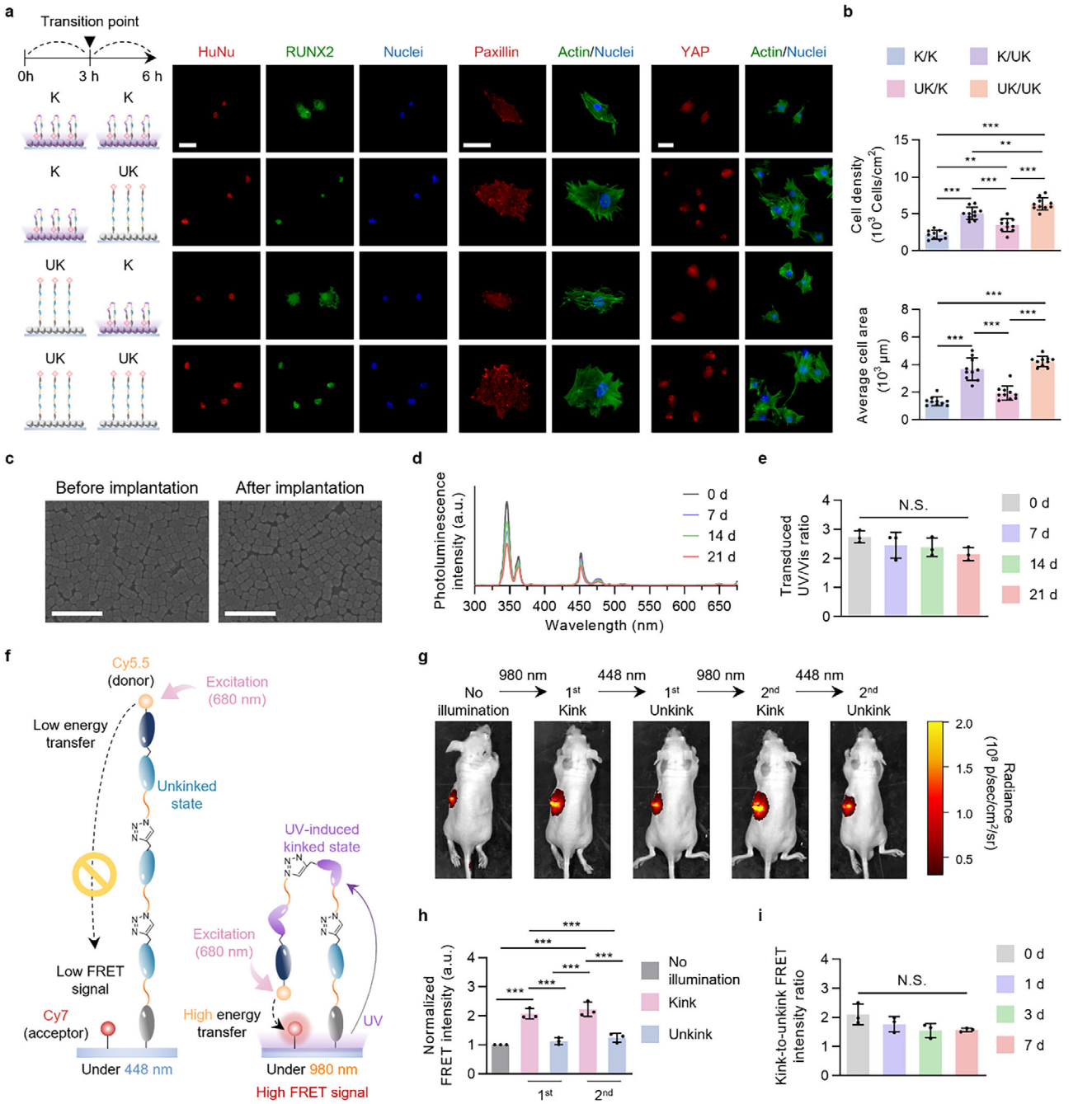

FIGURE 4 | Reversible multiple kinking and unkinking modulate the degree of ligand exposure in vivo. (a) Immunofluorescence images of RUNX2 along with human-targeted HuNu and nuclei, paxillin along with actin and nuclei, and YAP along with actin and nuclei of stem cells after 6 h of subcutaneous implantation of liganded tri-kink molecule-conjugated substrates with stem cells and (b) quantification of the density and average area of stem cells based on the images. Substrates in mice were illuminated with 980 nm ("K"; 1 W/cm^2 for 1 min) or 448 nm ("UK"; 0.2 W/cm^2 for 10 min)–-repeatedly ("K/K" and "UK/UK") or alternately ("K/UK" and "UK/K")–-at 0 h and 3 h after implantation. The data are presented as mean ± standard error ($n = 10$ randomly selected images from two independent substrates). (c) SEM images of the UCNT substrates before and 7 days after implantation. Scale bar: 1 μm. (d) Photoluminescence spectra of UCNT substrates collected from mice on days 0, 7, 14, and 21 after implantation upon 980 nm illumination and (e) upconverted emission intensity ratio of UV wavelength (highest intensity at 345 nm) to Vis light (highest intensity at 452 nm). The data are presented as mean ± standard error ($n = 3$ independent substrates). (f) Schematic representation of the mechanism of FRET-based confirmation of the kinked and unkinked states upon illumination at 980 and 448 nm, respectively, in vivo. When the donor-conjugated tri-kink molecules transition to the kinked state under 980 nm illumination, the distance between the donor and the acceptor on the UCNT surface decreases, enhancing energy transfer and resulting in a strong FRET signal. In the unkinked state under 448 nm illumination, the distance increases, preventing energy transfer and resulting in a weak FRET signal. (g) Images of FRET signals in live mice at 0 h after implantation during two cycles of 980 nm (1 W/cm^2 for 1 min) and 448 nm illumination (0.2 W/cm^2 for 10 min), and (h) quantification of FRET intensity, normalized to the intensity in the "No illumination" group. (i) FRET signal intensity ratio of the kinked state to the unkinked state on days 0, 1, 3, and 7 after implantation, calculated based on Figure S44. Asterisks indicate statistically significant differences with p-values (**$p < 0.01$ and ***$p < 0.001$), while N.S. represents statistically non-significant differences.

16163028, 2026, 86, Downloaded from https://advanced.onlinelibrary.wiley.com/doi/10.1002/adfm.77914 by Hanyang University Library, Wiley Online Library on [24/11/2026]. See the Terms and Conditions (https://onlinelibrary.wiley.com/terms-and-conditions) on Wiley Online Library for rules of use; OA articles are governed by the applicable Creative Commons License

under 680-nm irradiation to the substrate was measured using an in vivo imaging system. The FRET signal intensity was first measured in the absence of illumination and then after sequential illumination at 980 nm (1 W/cm^2 for 1 min) and 448 nm (0.2 W/cm^2 for 10 min), for two cycles. The kinked state induced by 980 nm illumination produced stronger FRET signals than the unkinked state induced by 448 nm illumination, and this pattern was consistently observed during the repeated measurements on day 0 after implantation (Figure 4g,h). The FRET signal was largely stable over 7 days after implantation as indicated by the maintenance of the FRET signal ratio in the kinked versus the unkinked state (Figures 4i and S44). Hematoxylin and eosin staining of subcutaneous tissue at the implant site and major organs indicated that liganded tri-kink molecule-UCNT substrate under 448 and 980 nm illumination was non-toxic (Figure S45). Consistently, monitored body weight loss remained below 10% of the initial body weight during the respective in vivo observation periods (Figure S46). This suggests that multiple kinking and unkinking in the tri-kink molecule-conjugated UCNT substrate through 980 nm and 448 nm illumination, respectively, can be used for tissue regeneration without exerting toxicity. Long-term investigation of functional tissue regeneration in vivo via a light-controllable tri-kink molecule-conjugated UCNT substrate is warranted to assess the actual therapeutic effect and non-toxicity in vivo.

3 | Conclusion

In this work, we introduced the novel concept of background component-free "multiple kinks" in the design of materials solely consisting of liganded multiple kink-bearing molecules with a tunable number of kink points (i.e., mono-kink, tri-kink, and penta-kink molecules), including flexible linkers, and densely packed via intermolecular interactions. Tri-kink molecules coupled to upconversion nanoparticle-coated materials mediated effective regulation of 980 nm light-triggered aromatic hydrogen bond-dominant kinking for ligand masking and 448 nm light-triggered π–π stacking-dominant unkinking for ligand exposure. The latter configuration cyclically stimulated integrin ligation and focal adhesion-mediated mechanotransduction and differentiation of stem cells in vitro and in vivo. We confirmed the maintenance of switchability between the kinked and unkinked states and upconverting functionality, as well as the absence of systemic toxicity in vivo.

Such regulation could not be achieved with mono-kink and penta-kink molecules, suggesting that the number of kink points is an important molecular design parameter for reversible ligand masking/exposure. This result is consistent with previous mono-kink-based materials, in which non-kink-bearing components were used together with mono-kink molecules to achieve dynamic ligand presentation. Because these materials contain additional background components, they make it difficult to isolate the contribution of multi-kink molecular structures to dynamic cell–material interactions. In contrast, surfaces composed solely of liganded multi-kink molecules provide a more direct platform for investigating how molecular kinking/unkinking regulates terminal ligand masking/exposure and downstream stem cell responses. Therefore, programming the repeat number, position, and sequence of kink points, as well as molecular length and ligand type, in liganded multi-kink molecules could offer useful modalities for the dynamic regulation of stem cell fate and early osteogenic responses in vivo, with potential relevance for future regenerative applications.

Acknowledgements

This work was supported by the National Research Foundation of Korea (NRF) grant funded by the Korea government (MSIT) (RS-2026-25494438). This research was also supported by the Nano & Material Technology Development Program through the National Research Foundation of Korea (NRF) funded by the Ministry of Science and ICT (RS-2024-00407234). This work was also supported by a Korea University Grant. HAADF-STEM imaging was conducted with the support of the Seoul Center in Korea Basic Science Institute (KBSI). The animal studies have been approved by the Animal Care and Use Committee of Korea Institute of Science and Technology (KIST), and all handling of mice was performed in accordance with the institutional regulations (KIST-IACUC-2025-12-010).

Conflicts of Interest

The authors declare no conflicts of interest.

Data Availability Statement

The data that support the findings of this study are available in the supplementary material of this article.

References

1. S. H. Northrup, "Molecular Mechanics of Kink Formation in Lipid Monolayers," *Journal of Physical Chemistry* 88 (1984): 3441–3446, https://doi.org/10.1021/j150660a015.

2. J. Widom, "Molecular Biology: DNA Bending and Kinking," *Nature* 309 (1984): 312–313, https://doi.org/10.1038/309312a0.

3. S. Kumar, B. Y. Ma, C. J. Tsai, H. Wolfson, and R. Nussinov, "Folding Funnels and Conformational Transitions via Hinge-Bending Motions," *Cell Biochemistry and Biophysics* 31 (1999): 141–164, https://doi.org/10.1007/BF02738169.

4. G. Woehlke and M. Schliwa, "Walking on Two Heads: the Many Talents of Kinesin," *Nature Reviews Molecular Cell Biology* 1 (2000): 50–58, https://doi.org/10.1038/35036069.

5. L. R. Ganser, M. L. Kelly, D. Herschlag, and H. M. Al-Hashimi, "The Roles of Structural Dynamics in The Cellular Functions of Rnas," *Nature Reviews Molecular Cell Biology* 20 (2019): 474–489, https://doi.org/10.1038/s41580-019-0136-0.

6. A. J. Roberts, T. Kon, P. J. Knight, K. Sutoh, and S. A. Burgess, "Functions and Mechanics of Dynein Motor Proteins," *Nature Reviews Molecular Cell Biology* 14 (2013): 713–726, https://doi.org/10.1038/nrm3667.

7. D. J. Klein, T. M. Schmeing, P. B. Moore, and T. A. Steitz, "The Kink-Turn: a New Rna Secondary Structure Motif," *EMBO journal* 20 (2001): 4214–4221, https://doi.org/10.1093/emboj/20.15.4214.

8. X. S. Shi, L. Huang, D. M. J. Lilley, P. B. Harbury, and D. Herschlag, "The Solution Structural Ensembles of RNA Kink-turn Motifs and Their Protein Complexes," *Nature Chemical Biology* 12 (2016): 146–152, https://doi.org/10.1038/nchembio.1997.

9. J. O. Streit, I. V. Bukvin, S. H. S. Chan, et al., "The Ribosome Lowers The Entropic Penalty of Protein Folding," *Nature* 633 (2024): 232–239, https://doi.org/10.1038/s41586-024-07784-4.

10. M. W. Macarthur and J. M. Thornton, "Influence of Proline Residues on Protein Conformation," *Journal of Molecular Biology* 218 (1991): 397–412, https://doi.org/10.1016/0022-2836(91)90721-H.

16163028, 2026, 86, Downloaded from https://advanced.onlinelibrary.wiley.com/doi/10.1002/adfm.77914 by Hanyang University Library, Wiley Online Library on [24/11/2026]. See the Terms and Conditions (https://onlinelibrary.wiley.com/terms-and-conditions) on Wiley Online Library for rules of use; OA articles are governed by the applicable Creative Commons License

11. S. C. R. Lummis, D. L. Beene, L. W. Lee, H. A. Lester, R. W. Broadhurst, and D. A. Dougherty, "Cis–Trans Isomerization at a Proline Opens the Pore of a Neurotransmitter-Gated Ion Channel," *Nature* 438 (2005): 248–252, https://doi.org/10.1038/nature04130.

12. J. Kim, S. Lee, Y. Kim, et al., "In Situ Self-Assembly for Cancer Therapy and Imaging," *Nature Reviews Materials* 8 (2023): 710–725, https://doi.org/10.1038/s41578-023-00589-3.

13. A. Naba, "Mechanisms of Assembly and Remodelling of the Extracellular Matrix," *Nature Reviews Molecular Cell Biology* 25 (2024): 865–885, https://doi.org/10.1038/s41580-024-00767-3.

14. T. G. Kapp, F. Rechenmacher, S. Neubauer, et al., "A Comprehensive Evaluation of the Activity and Selectivity Profile of Ligands for Rgd-Binding Integrins," *Scientific Reports* 7 (2017): 39805, https://doi.org/10.1038/srep39805.

15. R. Raman, G. Venkataraman, S. Ernst, V. Sasisekharan, and R. Sasisekharan, "Structural Specificity of Heparin Binding in the Fibroblast Growth Factor Family of Proteins," *Proceedings of the National Academy of Sciences* 100 (2003): 2357–2362, https://doi.org/10.1073/pnas.0437842100.

16. C. Debarnot, Y. R. Monneau, V. Roig-Zamboni, et al., "Substrate Binding Mode and Catalytic Mechanism of Human Heparan Sulfate D-Glucuronyl C5 Epimerase," *Proceedings of the National Academy of Sciences* 116 (2019): 6760–6765, https://doi.org/10.1073/pnas.1818333116.

17. M. K. Kan, F. Wang, J. M. Xu, J. W. Crabb, J. Z. Hou, and W. L. Mckeehan, "An Essential Heparin-Binding Domain in the Fibroblast Growth Factor Receptor Kinase," *Science* 259 (1993): 1918.

18. R. P. Richter, N. S. Baranova, A. J. Day, and J. C. F. Kwok, "Glycosaminoglycans in Extracellular Matrix Organisation: Are Concepts from Soft Matter Physics Key to Understanding the Formation of Perineuronal Nets?," *Current Opinion in Structural Biology* 50 (2018): 65–74, https://doi.org/10.1016/j.sbi.2017.12.002.

19. L. Sanz, L. García-Bermejo, F. J. Blanco, et al., "A Novel Cell Binding Site in the Coiled-Coil Domain of Laminin Involved in Capillary Morphogenesis," *EMBO Journal* 22 (2003): 1508–1517, https://doi.org/10.1093/emboj/cdg150.

20. Y. Mao and J. E. Schwarzbauer, "Fibronectin Fibrillogenesis, a Cell-Mediated Matrix Assembly Process," *Matrix Biology* 24 (2005): 389–399, https://doi.org/10.1016/j.matbio.2005.06.008.

21. K. P. Lu, G. Finn, T. H. Lee, and L. K. Nicholson, "Prolyl Cis-Trans Isomerization as a Molecular Timer," *Nature Chemical Biology* 3 (2007): 619–629, https://doi.org/10.1038/nchembio.2007.35.

22. J. D. Malcor, N. Ferruz, S. Romero-Romero, S. Dhingra, V. Sagar, and A. A. Jalan, "Deciphering the Folding Code of Collagens," *Nature Communications* 16 (2025): 2702, https://doi.org/10.1038/s41467-024-54046-y.

23. A. Forlino, D. R. Keene, K. Schmidt, and J. C. Marini, "An A2(I) Glycine to Aspartate Substitution Is Responsible for the Presence of a Kink in Type I Collagen in a Lethal Case of Osteogenesis Imperfecta," *Matrix Biology* 17 (1998): 575–584, https://doi.org/10.1016/S0945-053X(98)90109-3.

24. K. Beck, V. C. Chan, N. Shenoy, A. Kirkpatrick, J. A. M. Ramshaw, and B. Brodsky, "Destabilization of Osteogenesis Imperfecta Collagen-Like Model Peptides Correlates with the Identity of the Residue Replacing Glycine," *Proceedings of the National Academy of Sciences* 97 (2000): 4273–4278, https://doi.org/10.1073/pnas.070050097.

25. D. J. Behonick, Z. Q. Xing, S. Lieu, et al., "Role of Matrix Metalloproteinase 13 in both Endochondral and Intramembranous Ossification during Skeletal Regeneration," *PLoS ONE* 2 (2007): 1150.

26. K. L. Lin, D. W. Zhang, M. H. Macedo, W. G. Cui, B. Sarmento, and G. F. Shen, "Advanced Collagen-Based Biomaterials for Regenerative Biomedicine," *Advanced Functional Materials* 29 (2019): 1804943, https://doi.org/10.1002/adfm.201804943.

27. J. K. Mouw, G. Q. Ou, and V. M. Weaver, "Extracellular Matrix Assembly: a Multiscale Deconstruction," *Nature Reviews Molecular Cell Biology* 15 (2014): 771–785, https://doi.org/10.1038/nrm3902.

28. P. Kannus, "Structure of the Tendon Connective Tissue," *Scandinavian Journal of Medicine & Science in Sports* 10 (2000): 312–320, https://doi.org/10.1034/j.1600-0838.2000.010006312.x.

29. M. Franchi, A. Trirè, M. Quaranta, E. Orsini, and V. Ottani, "Collagen Structure of Tendon Relates to Function," *Scientific World Journal* 7 (2007): 404–420, https://doi.org/10.1100/tsw.2007.92.

30. N. H. Cho, A. Guerrero-Martínez, J. S. C. Ma, et al., "Bioinspired Chiral Inorganic Nanomaterials," *Nature Reviews Bioengineering* 1 (2023): 88–106, https://doi.org/10.1038/s44222-022-00014-4.

31. S. I. S. Hendrikse, R. Contreras-Montoya, A. Ellis, P. Thordarson, and J. W. Steed, "Biofunctionality with a Twist: the Importance of Molecular Organisation, Handedness and Configuration in Synthetic Biomaterial Design," *Chemical Society Reviews* 51 (2022): 28–42, https://doi.org/10.1039/D1CS00896J.

32. K. Debnath, K. L. Heras, A. Rivera, S. Lenzini, and J. W. Shin, "Extracellular Vesicle–Matrix Interactions," *Nature Reviews Materials* 8 (2023): 390–402, https://doi.org/10.1038/s41578-023-00551-3.

33. S. H. Yang, M. Wang, D. W. Tian, et al., "Dna-Functionalized Artificial Mechanoreceptor for De Novo Force-Responsive Signaling," *Nature Chemical Biology* 20 (2024): 1066–1077, https://doi.org/10.1038/s41589-024-01572-x.

34. W. X. Wang, W. Chen, C. Y. Wu, et al., "Hydrogel-Based Molecular Tension Fluorescence Microscopy for Investigating Receptor-Mediated Rigidity Sensing," *Nature Methods* 20 (2023): 1780–1789, https://doi.org/10.1038/s41592-023-02037-0.

35. Y. S. Hu, J. Rogers, Y. X. Duan, et al., "Quantifying T Cell Receptor Mechanics at Membrane Junctions Using Dna Origami Tension Sensors," *Nature Nanotechnology* 19 (2024): 1674–1685, https://doi.org/10.1038/s41565-024-01723-0.

36. W. B. He, J. X. Bai, X. Chen, et al., "Reversible Dougong Structured Receptor–Ligand Recognition for Building Dynamic Extracellular Matrix Mimics," *Proceedings of the National Academy of Sciences* 119 (2022): 2117221119, https://doi.org/10.1073/pnas.2117221119.

37. M. Centola, E. Poppleton, S. Ray, et al., "A Rhythmically Pulsing Leaf-Spring Dna-Origami Nanoengine That Drives A Passive Follower," *Nature Nanotechnology* 19 (2024): 226–236, https://doi.org/10.1038/s41565-023-01516-x.

38. Y. W. Hu, Y. J. Ke, and I. Willner, "A pH-Cascaded DNA Hydrogel Mediated by Reconfigurable A-motif Duplex, i-Motif Quadruplex, and T·A-T Triplex Structures," *Advanced Functional Materials* 33 (2023): 2304966, https://doi.org/10.1002/adfm.202304966.

39. W. Li, Z. Yan, J. Ren, and X. Qu, "Manipulating Cell Fate: Dynamic Control of Cell Behaviors on Functional Platforms," *Chemical Society Reviews* 47 (2018): 8639–8684, https://doi.org/10.1039/C8CS00053K.

40. J. Gemen, J. R. Church, T. P. Ruoko, et al., "Disequilibrating Azobenzenes by Visible-Light Sensitization under Confinement," *Science* 381 (2023): 1357–1363, https://doi.org/10.1126/science.adh9059.

41. X. Z. Wang, A. Kerckhoffs, J. Riexinger, et al., "On–Off Nanopores for Optical Control of Transmembrane Ionic Communication," *Nature Nanotechnology* 20 (2025): 432–440, https://doi.org/10.1038/s41565-024-01823-x.

42. P. Leippe, P. Donthamsetti, T. Ko, C. Stanley, E. Isacoff, and D. Trauner, "Cell-Specific Optical Control of Ampa Glutamate Receptors with a Photoswitchable Tethered Antagonist," *Angewandte Chemie International Edition* 63 (2024): 202411181, https://doi.org/10.1002/anie.202411181.

43. Y. Kim, R. Thangam, J. Yoo, et al., "Photoswitchable Microgels for Dynamic Macrophage Modulation," *Advanced Materials* 34 (2022): 2205498, https://doi.org/10.1002/adma.202205498.

16163028, 2026, 86, Downloaded from https://advanced.onlinelibrary.wiley.com/doi/10.1002/adfm.77914 by Hanyang University Library, Wiley Online Library on [24/11/2026]. See the Terms and Conditions (https://onlinelibrary.wiley.com/terms-and-conditions) on Wiley Online Library for rules of use; OA articles are governed by the applicable Creative Commons License

44. T. Mashita, T. Kowada, H. Yamamoto, et al., "Quantitative Control of Subcellular Protein Localization with a Photochromic Dimerizer," *Nature Chemical Biology* 20 (2024): 1461–1470, https://doi.org/10.1038/s41589-024-01654-w.

45. X. Y. Zhang, S. Dhir, L. Melidis, et al., "optical Control of Gene Expression Using a dna G-quadruplex Targeting Reversible Photoswitch," *Nature Chemistry* 17 (2025): 875–882, https://doi.org/10.1038/s41557-025-01792-1.

46. L. F. Kadem, K. G. Suana, M. Holz, et al., "High-Frequency Mechanostimulation of Cell Adhesion," *Angewandte Chemie International Edition* 56 (2017): 225–229, https://doi.org/10.1002/anie.201609483.

47. J. E. Hein and V. V. Fokin, "Copper-catalyzed Azide–alkyne Cycloaddition (CuAAC) and Beyond: New Reactivity of Copper(i) Acetylides," *Chemical Society Reviews* 39 (2010): 1302, https://doi.org/10.1039/b904091a.

48. D. Huang, Y. Liu, A. Qin, and B. Tang, "Recent Advances in Alkyne-based Click Polymerizations," *Polymer Chemistry* 9 (2018): 2853–2867, https://doi.org/10.1039/C7PY02047C.

49. R. Trihan, A. Aimable, M. Lejeune, P. Andreazza, X. Cattoen, and F. Rossignol, "Highly Efficient Consolidation of Mesoporous Silica Microstructures Using Photonic Curing," *Advanced Functional Materials* 34 (2024): 2315973.

50. L. D. Trucco, P. A. Mundra, K. Hogan, et al., "Ultraviolet Radiation–induced DNA Damage Is Prognostic for Outcome in Melanoma," *Nature Medicine* 25 (2019): 221–224, https://doi.org/10.1038/s41591-018-0265-6.

51. L. M. Jin, X. Chen, C. K. Siu, F. Wang, and S. F. Yu, "Enhancing Multiphoton Upconversion from NaYF 4: Yb/Tm@NaYF 4 Core–Shell Nanoparticles via the Use of Laser Cavity," *ACS Nano* 11 (2017): 843–849, https://doi.org/10.1021/acsnano.6b07322.

52. J. S. Huang, L. Yan, S. B. Liu, N. Song, Q. Y. Zhang, and B. Zhou, "Dynamic Control of Orthogonal Upconversion in MigratoryCore–Shell Nanostructure toward Information Security," *Advanced Functional Materials* 31 (2021): 2009796, https://doi.org/10.1002/adfm.202009796.

53. A. Schroter, S. Märkl, N. Weitzel, and T. Hirsch, "Upconversion Nanocrystals with High Lanthanide Content: Luminescence Loss by Energy Migration versus Luminescence Enhancement by Increased NIR Absorption," *Advanced Functional Materials* 32 (2022): 2113065, https://doi.org/10.1002/adfm.202113065.

54. S. H. Wen, J. J. Zhou, K. Z. Zheng, A. Bednarkiewicz, X. G. Liu, and D. Y. Jin, "Advances in Highly Doped Upconversion Nanoparticles," *Nature Communications* 9 (2018): 2415, https://doi.org/10.1038/s41467-018-04813-5.

55. E. Ureña-Horno, K. Liu, and M. Giardiello, "Controllable and Tuneable Growth of $NaYbF_4$: Tm(0.5%)Fe(5%)@Na(Yb/Y)F_4 -core@Shell Structures and the Effect of Their Geometry on Upconversion Luminescence," *Journal of Materials Chemistry C* 11 (2023): 12356–12363, https://doi.org/10.1039/D3TC01215H.

56. R. Ellerbrock, M. Stein, and J. Schaller, "Comparing Amorphous Silica, Short-range-ordered Silicates and Silicic Acid Species by FTIR," *Scientific Reports* 12 (2022): 11708, https://doi.org/10.1038/s41598-022-15882-4.

57. A. M. Cortizas and O. López-Costas, "Linking Structural and Compositional Changes in Archaeological human Bone Collagen: an FTIR-ATR Approach," *Scientific Reports* 10 (2020): 17888, https://doi.org/10.1038/s41598-020-74993-y.

58. R. Javier-Astete, J. Melo, J. Jimenez-Davalos, and G. Zolla, "Classification of Amazonian Fast-growing Tree Species and Wood Chemical Determination by FTIR and Multivariate Analysis (PLS-DA, PLS)," *Scientific Reports* 13 (2023): 7827, https://doi.org/10.1038/s41598-023-35107-6.

59. K. Soongprasit, V. Sricharoenchaikul, and D. Atong, "Phenol-derived Products from Fast Pyrolysis of Organosolv Lignin," *Energy Reports* 6 (2020): 151–167, https://doi.org/10.1016/j.egyr.2020.08.040.

60. S. T. Song, L. L. Wang, J. Su, et al., "Manifold Dynamic Non-covalent Interactions for Steering Molecular Assembly and Cyclization," *Chemical Science* 12 (2021): 11659–11667, https://doi.org/10.1039/D1SC03733A.

61. Y. G. Zhang, X. W. Xie, J. L. Liu, et al., "Ionic Liquids with Reversible Photo-induced Conductivity Regulation in Aqueous Solution," *Scientific Reports* 13 (2023): 13766, https://doi.org/10.1038/s41598-023-40905-z.

62. J. X. Meng, G. Yang, L. Liu, Y. Y. Song, L. Jiang, and S. T. Wang, "Cell Adhesive Spectra along Surface Wettability Gradient from Superhydrophilicity to Superhydrophobicity," *Science China Chemistry* 60 (2017): 614–620, https://doi.org/10.1007/s11426-016-9031-8.

63. X. K. Yao, C. Qi, C. R. Sun, F. W. Huo, and X. Q. Jiang, "Poly(ethylene glycol) Alternatives in Biomedical Applications," *Nano Today* 48 (2023): 101738, https://doi.org/10.1016/j.nantod.2022.101738.

64. M. N. Han, T. Honda, D. Ishikawa, E. Ito, M. Hara, and Y. Norikane, "Realization of Highly Photoresponsive Azobenzene-functionalized Monolayers," *Journal of Materials Chemistry* 21 (2011): 4696, https://doi.org/10.1039/c0jm03697h.

65. W. Zhang, C. H. Lu, M. L. Nakamoto, et al., "Curved Adhesions Mediate Cell Attachment to Soft Matrix Fibres in Three Dimensions," *Nature Cell Biology* 25 (2023): 1453–1464, https://doi.org/10.1038/s41556-023-01238-1.

66. B. K. K. Teo, S. T. Wong, C. K. Lim, et al., "Nanotopography Modulates Mechanotransduction of Stem Cells and Induces Differentiation through Focal Adhesion Kinase," *ACS Nano* 7 (2013): 4785–4798, https://doi.org/10.1021/nn304966z.

67. N. Munding, M. Fladung, Y. Chen, et al., "Bio-Metamaterials for Mechano-Regulation of Mesenchymal Stem Cells," *Advanced Functional Materials* 34 (2024): 2301133, https://doi.org/10.1002/adfm.202301133.

68. S. J. Attwood, E. Cortes, A. W. M. Haining, et al., "Adhesive Ligand Tether Length Affects the Size and Length of Focal Adhesions and Influences Cell Spreading and Attachment," *Scientific Report* 6 (2016): 34334, https://doi.org/10.1038/srep34334.

69. D. S. H. Wong, J. N. Li, X. H. Yan, et al., "Magnetically Tuning Tether Mobility of Integrin Ligand Regulates Adhesion, Spreading, and Differentiation of Stem Cells," *Nano Letters* 17 (2017): 1685–1695, https://doi.org/10.1021/acs.nanolett.6b04958.

70. B. Trappmann, J. E. Gautrot, J. T. Connelly, et al., "Extracellular-matrix Tethering Regulates Stem-cell Fate," *Nature Materials* 11 (2012): 642–649, https://doi.org/10.1038/nmat3339.

71. K. H. Vining and D. J. Mooney, "Mechanical Forces Direct Stem Cell Behaviour in Development and Regeneration," *Nature Reviews Molecular Cell Biology* 18 (2017): 728–742, https://doi.org/10.1038/nrm.2017.108.

72. J. P. Conboy, I. I. Petitjean, A. van der Net, and G. H. Koenderink, "How Cytoskeletal Crosstalk Makes Cells Move: Bridging Cell-Free and Cell Studies," *Biophysical Reviews* 5 (2024): 021307.

73. A. K. Gaharwar, I. Singh, and A. Khademhosseini, "Engineered Biomaterials for in Situ Tissue Regeneration," *Nature Reviews Materials* 5 (2020): 686–705, https://doi.org/10.1038/s41578-020-0209-x.

74. K. Min, S. K. Karuppannan, and G. Tae, "The Impact of Matrix Stiffness on Hepatic Cell Function, Liver Fibrosis, and Hepatocellular Carcinoma—Based on Quantitative Data," *Biophysical Reviews* 5 (2024): 021306.

75. R. Roy, S. Hohng, and T. Ha, "A Practical Guide to Single-molecule FRET," *Nature Methods* 5 (2008): 507–516, https://doi.org/10.1038/nmeth.1208.

Supporting Information

Additional supporting information can be found online in the Supporting Information section.

Supporting File: adfm77914-sup-0001-SuppMat.pdf.

16163028, 2026, 86, Downloaded from https://advanced.onlinelibrary.wiley.com/doi/10.1002/adfm.77914 by Hanyang University Library, Wiley Online Library on [24/11/2026]. See the Terms and Conditions (https://onlinelibrary.wiley.com/terms-and-conditions) on Wiley Online Library for rules of use; OA articles are governed by the applicable Creative Commons License